J Solid State Electrochem (2012) 16:1453–1460
DOI 10.1007/s10008-011-1525-2

ORIGINAL PAPER

Preparation and characterization of silicon monoxide/graphite/carbon nanotubes composite as anode for lithium-ion batteries

Yurong Ren · Jianning Ding · Ningyi Yuan · Shuyong Jia · Meizhen Qu · Zuolong Yu

Received: 12 May 2011 / Revised: 1 August 2011 / Accepted: 5 August 2011 / Published online: 27 September 2011

Abstract Silicon monoxide/graphite/multi-walled carbon nanotubes (SiO/G/CNTs) material was prepared by ball milling followed by chemical vapor deposition method and characterized by X-ray diffraction, scanning electron microscopy (SEM), galvanostatic charge–discharge, and AC impedance spectroscopy, respectively. The results revealed that SiO/G/CNTs exhibited an initial specific discharge capacity of 790 mAh g^{-1} with a columbic efficiency of 65%. After 100 cycles, a high reversible capacity of 495 mAh g^{-1} is still retained. The improved electrochemical properties were due to beneficial SEI by the SEM and EIS results.

Keywords Silicon monoxide · Graphite · In situ grown · Chemical vapor deposition · Anode · Li-ion battery

Introduction

Carbonaceous materials have been widely used as anode materials for Li-ion batteries because of their high-initial columbic efficiency and good cyclic stability [1–4]. However, new anode materials with higher discharge capacity and better reversibility capacity are still strongly demanded for expanding applications to the large energy-consuming devices such as electric vehicles and other various digital portable equipments of next generation [5, 6]. Silicon is considered as one of the most attractive candidate anode materials and widely investigated due to its high theoretical specific capacity of 4,200 mAh g^{-1}, corresponding to the fully lithiated composition of $Li_{4.4}Si$, which is ten-fold higher than that of graphite [7–9]. Nevertheless, Si has not been commercially applied so far due to its poor cycleability. The large volumetric expansion during charge (as much as 400% expansion from the initial volume) leads to the internal cracks of its particles and then damaging the electrode, which would greatly increase electric resistivity of the electrode. Apparently, the defect occurs by poor contacts among Si particles as well as Si particles and current collector when cycling [5, 10]. For this reason, lots of considerations have been made to overcome such problem during the last two decades, such as amorphous Si thin film coating [11], Si–carbon or SiO–carbon composites with mechanical mixing [6, 12–14], carbon pyrolysis on the Si surface [15–18] and Si–carbon–carbon nanotube composites [19–21], and so on. However, such measures still face some old issues of unsatisfied cycleability, complicated synthetic processes, which are unsuitable for mass production, and high relatively cost to bring commercialization.

Carbon nanotubes (CNTs) have received considerable interest as Li insertion host materials since their discovery in 1991 [22]. Although CNTs in general, as reported in the literatures are known to exhibit a higher reversible capacity than graphite [23–29], a high irreversible loss and a large-voltage hysteresis are commonly observed, which greatly limit their application as anode material in Li-ion battery.

Y. Ren · J. Ding (✉) · N. Yuan
Center for Low-Dimensional Materials,
Micro-nano Devices and System, Changzhou University,
Changzhou 213164, China
e-mail: ryrchem@cczu.edu.cn

Y. Ren
e-mail: ryrchem@163.com

S. Jia
Changzhou Institute of Chemistry,
Changzhou 213164, China

M. Qu · Z. Yu
Chengdu Institute of Organic Chemistry,
Chinese Academy of Sciences,
Chengdu 610041, China

Nevertheless, CNTs have been proved to be a better choice over graphite as a matrix material for Li-ion battery due to their excellent physical properties including superior mechanical strength (Young's modulus ~1.0 TPa) [30] and electrical conductivity (resistivity $<10^{-4}$ Ω cm) [31] in comparison to any of the existing materials known to date. They also possess a large aspect ratio, structural flexibility, as well as tortuosity [32].

In the present work, metallic silicon monoxide particles (SiO) which have an average size of 2–3 μm and modified graphite (G) spheres which have an average of 16 μm were selected as starting materials and modified to provide more suitable anodic material for Li-ion batteries through the novel compositeness with multi-walled carbon nanotubes (MWCNTs). The MWCNT (growth) on SiO or SiO/G particles was prepared on the basis of following two steps: step 1, SiO and graphite particles were milled using a planetary ball mill; step 2, MWCNTs were grown on the surface of SiO or SiO/G particles during chemical vapor deposition (CVD). The effect of MWCNTs coatings on the surface of SiO or SiO/G particles on the electrochemical performance such as capacity, cycleability, and the characteristics of the solid electrolyte interface (SEI) on the surface of carbon nanotubes were investigated in details.

Experimental

Preparation of composite material

Equal proportions of silicon monoxide (SiO, 99.99%, Shanghai Chemical Co. Ltd., China) and graphite (Shanghai Shanshan Tech Co., Ltd, China, 16 μm) were placed together with stainless steel (SS) balls in a 100-ml SS vial. The weight ratio of the SS ball to the raw materials was maintained at 12:1 and the vial was filled with argon gas. The mixed powders were milled for 18 h at 350 rpm, and then SiO/G samples were collected.

A 1.8-g Ni $(NO_3)_3{\cdot}6H_2O$ (1.8 g, A.R) and 10 g SiO/G composite powder were added into 50-ml ethanol, and the slurry was stirred for 3 h at room temperature to impregnate Ni $(NO_3)_3{\cdot}6H_2O$ on the surface of SiO/G powder. After ethanol was removed using rotary evaporator at 338 K, the obtained precursor was dried at 378 K for 6 h under vacuum. The mass ratio of Ni $(NO_3)_3{\cdot}6H_2O$ to SiO/G powder is 3 wt.%. The dried specimen inserted into a fixed-bed reactor (quartz tube of 38 mm of inner diameter and 100 cm of length with a horizontal electric furnace) was heated up to 873 K at a heating rate of 10 K min^{-1} under N_2 atmosphere (200 ml min^{-1}), and upon reaching the temperature, the flow was changed with N_2 and H_2 mixed gas (H_2/N_2=1/4 volume, total flow 200 ml min^{-1}) for 30 min. As follow, the mixed gas of CH_4 and H_2 (CH_4/H_2= 4/1 volume, total flow 200 ml min^{-1}) were introduced over SiO/G powder for another 60 min. After the CNTs growth, the reactor was cooled down to room temperature in He flow. The amount of CNTs was carefully controlled to be 30 wt.% of the weight of the composite SiO/G powder. The as-prepared composite product was denoted as SiO/G/CNTs.

Characterization

Powder X-ray diffraction (XRD) data were obtained by a Philips X-Pert system (Cu–Kα radiation). The morphology of as-prepared product were observed using scanning electron microscope (SEM, JEOL 5900LV) and transmission electron microscope (TEM, JEM-100CX). In addition, morphology change of electrode after cycles was also collected by SEM.

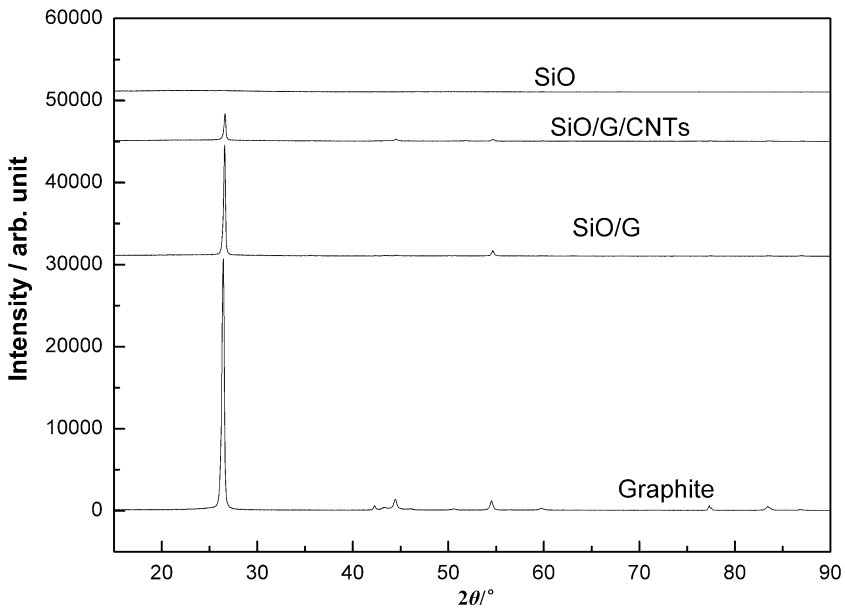

Fig. 1 XRD patterns of samples: *SiO*, *Graphite*, *SiO/G*, and *SiO/G/CNTs*

Electrochemcial measurements

The electrochemical test was using CR2016 coin-type half-cell. The electrode was prepared by casting an aqueous slurry containing 85 wt.% active powder, 5 wt.% carbon black (super P), and 10 wt.% carboxymethyl cellulose (CMC, A.R) as a binder, onto a copper foil (16-μm thick). The electrodes were then dried at 378 K under vacuum for 12 h, pressed using roll-type mill under 100 MPa. The electrolyte was 1 mol l^{-1} LiPF6 in EC/DMC/EMC (1:1:1, *v/v/v*) mixed solvents. The cells were assembled in an argon-filled glove box using a metallic lithium foil as a counter electrode. The discharge–charge test was carried out on a Kingtian system. The cells were discharged/charged between 0.02 and 1.5 V versus Li/Li^+ at a constant current density of 230 mA g^{-1}. Electrochemical impedance spectroscopy (EIS) measurements of electrode after given cycles were carried out at M283 electrochemical work station (USA, EG&G Corporation) over the frequency range from 100 kHz to 100 MHz with an amplitude of 5 mV.

Results and discussion

Material characterization

XRD profiles of SiO particles, graphite, SiO/G and SiO/G/CNTs are shown in Fig. 1 As observed, graphite using in

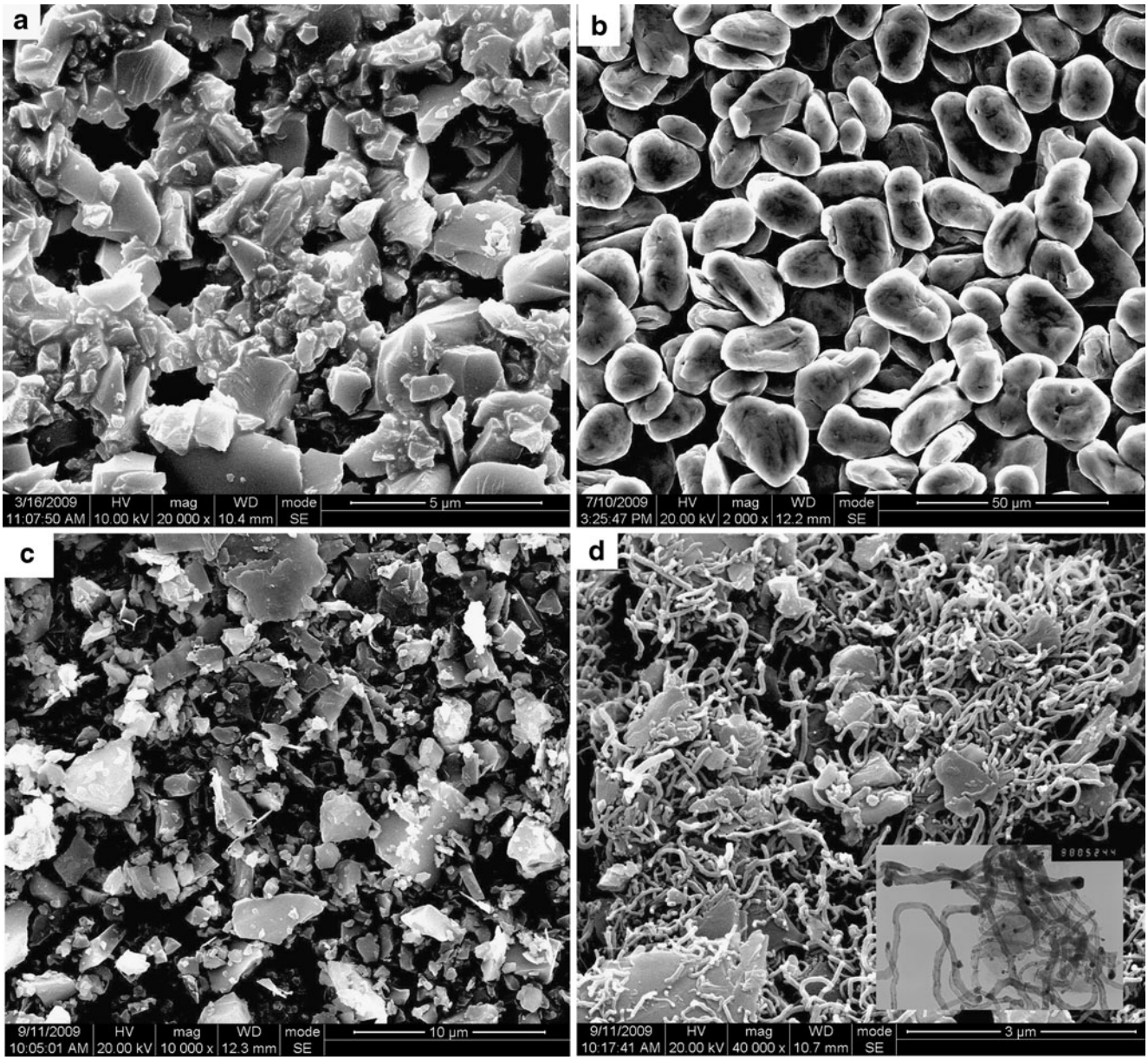

Fig. 2 SEM micrographs of samples: **a** SiO, **b** graphite, **c** SiO/G, and **d** CNTs-coated SiO/G; TEM image of SiO/G/CNTs was inserted

this paper is crystalline, whereas SiO is amorphous [33]. The pattern for milled SiO/G sample shows that the peak corresponding to graphite decreases after ball milling. Meantime, no any new peak is observed. The XRD pattern of SiO/G/CNTs composites has three diffraction peaks of CNTs at about 26.0°, 43.5°, and 54.5°, indexed with 002, 100, and 004 diffraction planes of hexagonal graphite (JCPDS card files, No. 41–1487), respectively.

Figure 2 shows the SEM images of different samples. The SEM images of the silicon monoxide and modified graphite sphere, used to prepare the SiO/G and SiO/G/CNTs composite material, are also presented. As can be seen, SiO powders show a uniform distribution with the average particle diameter of about 3 μm. The overall particle shape of graphite was spheroidicity. Figure 2c shows that SiO is homogeneously distributed in graphite matrix, which would provide a buffer during the insertion/extraction of lithium ions, and SiO/G particles are coated by the CNTs. After coating, the particles become more agglomerate and the edges become less discernable. The CNTs tubular morphology was further characterized by TEM. Figure 2d reveals CNTs grow on the surface of SiO/G particles in SiO/G/CNTs composites, while the SiO/G particles are enwrapped by the CNTs cage. The CNTs layer possesses a large amount of cavity void as the CNTs themselves carry a coiled shape. It is clearly seen that the surface of the particles is coated with a homogeneous layer, which comprises a large number of uniformly distributed protrudes of MWCNTs and the tube wall is smooth.

Electrochemical performance of SiO/G and SiO/G/CNTs

The discharge/charge curves of SiO/G and SiO/G/CNTs composite materials are shown in Fig. 3. During the first insertion process, SiO/G and SiO/G/CNTs electrode present a distinct plateau at around 0.20–0.02 V, which is mainly caused by the alloying process of silicon with lithium and the insertion of lithium ions into the carbon host. The slope at about 0.8–0.45 V corresponds to the irreversible decomposition of electrolyte on the surface of CNTs and (or) SiO/G particles, which results in the formation of SEI film on the electrode surface. It was approved in the company that this plateau disappears in the subsequent cycles. During the first-charge process, the broad plateau at around 0.4 V corresponds to the dealloying reaction of lithium from the LixSi phase. However, SiO/G and SiO/G/CNTs display obvious differences in terms of charge–discharge curves. Compared to SiO/G, SiO/G/CNTs electrode demonstrates a lower intercalation voltage plateau and a higher-extraction voltage plateau in the first cycle, which should be responsible for the reduced charge/discharge capacity of SiO/G/CNTs electrode. Moreover, the potential and the length of plateaus for two electrodes present different change with cycles. From the second cycle to the sixtieth

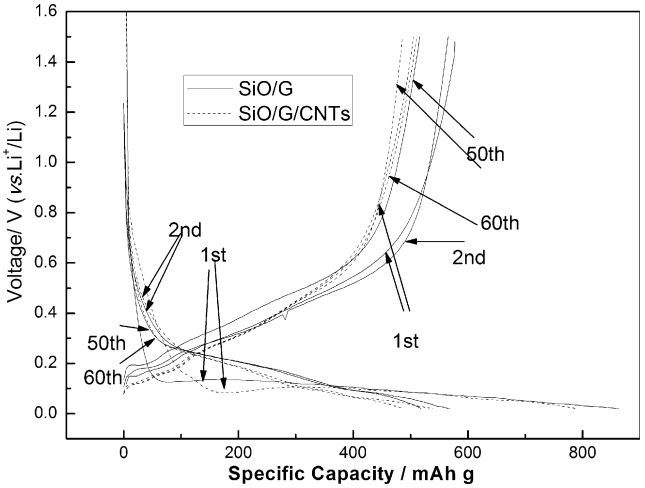

Fig. 3 Charge–discharge curves of SiO/G for first, second, and fiftieth cycle and CNT-coated SiO/G electrode for first, second, and sixtieth cycle

cycle, the potential difference between lithium insertion and lithium extraction plateau of SiO/G/CNTs electrode decreases, while the length of plateau increases. However, the potential difference of SiO/G electrode decreases and then increase with the increasing of cycle number. In the fiftieth cycle, the potential difference between lithium insertion and lithium extraction of SiO/G electrode is much larger than that of CNTs-coated SiO/G electrode and the length of its plateaus decrease largely. These results prove that the conductive network of SiO/G/CNTs electrode is maintained during the prolonged cycling, while the microstructure of SiO/G electrode is destroyed severely. This is consistent with the cycle performance of SiO/G/CNTs electrode.

Figure 4 depicts the differential capacity plot of SiO/G/CNTs composite at the first, second, and sixtieth cycle. It can be seen that Si and carbon are active materials. In the

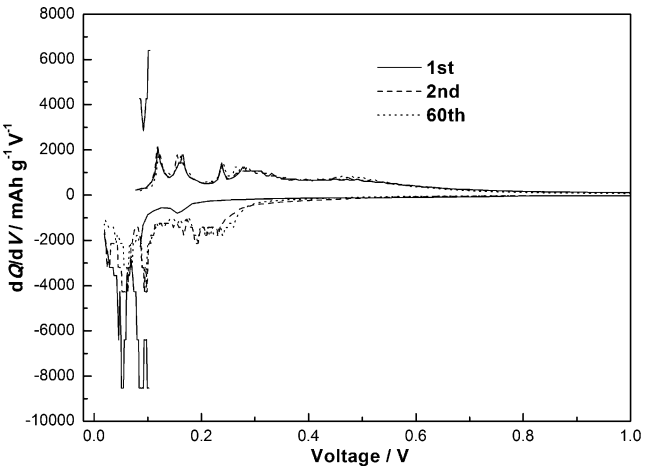

Fig. 4 Differential capacity vs. voltage curves of CNT-coated SiO/G/DC electrode for first, second, and sixtieth cycle

first cycle, the reduction peak at 0.05 V corresponds to the lithium insertion reaction into nanocrystalline Si, while the oxidation peaks at 0.25 and 0.48 V are lithium extraction reaction from LixSi. There are peaks due to graphite and carbon nanotube at 0.157, 0.08, 0.05 0.1, and 0.16 V, respectively. After the first cycle, the peaks for graphite have no significant change except of lithium insertion peak shifting positively 14 mV. The peak intensity due to the reaction of Li ion with amorphous Si does not decrease even after the sixtieth cycle, which suggests the excellent capacity retention of the composite.

Figure 5 shows the variation of specific capacity versus cycle number of SiO/G and SiO/G/CNTs cycled at a current density of 230 mA g^{-1}. The SiO/G electrode delivers an initial discharge capacity of 855 mAh g^{-1} with an irreversible loss of 284 mAh g^{-1}. However, it shows poor capacity retention ability. After 50 cycles, the reversible capacity retains only 390 mAh g^{-1}, with capacity loss of about 55%. In contrast, SiO/G/CNTs composite exhibits much better capacity retention. The first discharge and charge capacity is 790 mAh g^{-1} and 513 mAh g^{-1}, respectively. The SiO/G/CNTs composite electrode reveals a rechargeable capacity of above 495 mAh g^{-1} for nearly 100 cycles and the reversible capacity retention is more than 96.5% and the reversible capacity retention is 487 mAh g^{-1} after 130 cycles. The columbic efficiency of the composite increases from 65% to over 99% during the initial 3 cycles and remains above 99% in subsequent cycles. The SiO/G/CNTs composite electrode demonstrates much better electrochemical performance than SiO/G electrodes. When SiO reacts with lithium, there is a dramatic volume expansion, inducing cracking and pulverization. By embedding SiO and/or SiO/G particles in carbon nanotubes matrix, the volume expansion and contraction of SiO and/or SiO/G particles can be effectively buffered by the flexible carbon nanotubes. In addition, carbon nanotubes also provide a highly conductive medium for electron transfer during the lithiation and delithiation process. That is why the composite material shows improved cycling stability. And it is supposed that the better SEI layers are formed on the surface of SiO/G/CNTs electrode.

In order to shed the most light on the enhanced electrochemical performance of material via coating, the morphological change of the composite electrodes after different cycles were examined by SEM (Fig. 6). After the first cycle, obvious difference of the surfaces of SiO/G and SiO/G/CNTs electrode is observed. As shown in Fig. 6a, b, relatively homogeneous and compact SEI layers are observed on the surface of SiO/G/CNTs electrode and no crack appears for comparison. Moreover, the integrity of SiO/G/CNTs electrode is preserved. During the repeated alloying and dealloying, the SiO/G/CNTs electrode is still stable and stands up to the volume change of silicon. After 50 cycles, there is no significant change in the microstructure of SiO/G/CNTs composite electrode (Fig. 6d), while large fracture appears in SiO/G electrode (Fig. 6c). These results indicate that carbon nanotubes coating play a significant role in forming compact SEI layer and protects the integrity of the electrode structure. Since the final SiO/G composite was ground by ball milling, it was unavoidable that some monoxide silicon and graphite particles were bared on the surface of SiO/G composite. It was reported that when the silicon particles contact with the electrolyte directly, polymer-like porous substance will be formed on the surface of silicon particles, which prevents the formation of SEI passivation layer on the silicon surface [34]. In contrast, stable SEI layers may be formed since carbon nanotubes coating on Si/G composite prevent silicon from exposing to

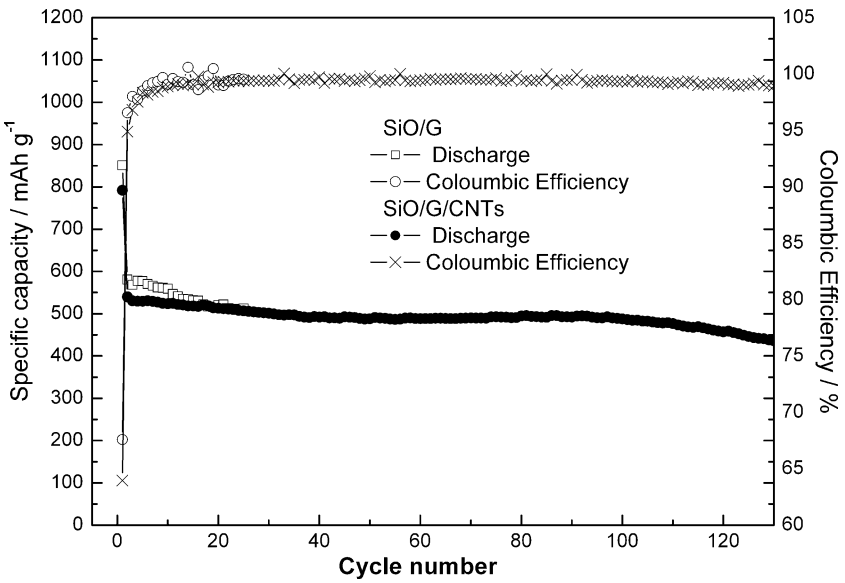

Fig. 5 Specific capacity vs. cycle number of SiO/G and SiO/G/CNTs cycled

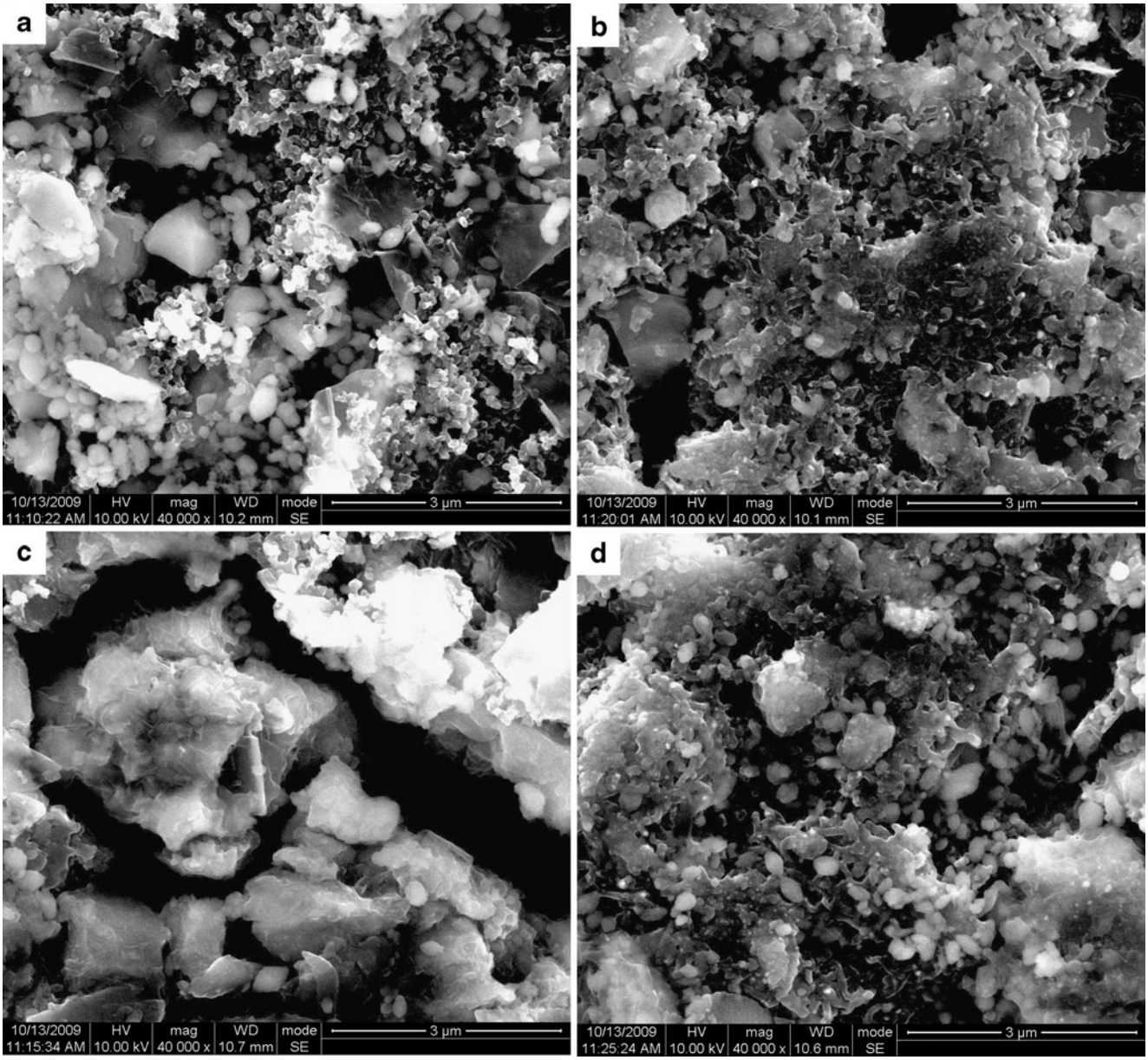

Fig. 6 SEM images of composite electrode. SiO/G: after first cycle (**a**) and after fiftieth cycle (**c**). SiO/G/CNTs: after first cycle (**b**) and after sixtieth cycle (**d**)

electrolyte. Therefore, the improved cyclic performance of SiO/G/CNTs composite is attributed to the fact that carbon nanotubes decrease the degree of lithium insertion into electrode materials and ameliorate the surface characteristics of SiO/G.

To further understand the reason for the improved cycleability of the SiO/G/CNTs composite electrode, EIS of SiO/G and SiO/G/CNTs composite material electrodes in the open circuirt potential before and after cycling was compared in Fig. 7. As shown, all of the Nyquist plots consist of one depressed semicircle at high frequencies (HF) and a straight line at low frequencies (LF). Semicircle with the active substance particles charge-transfer resistance between the units corresponds to slash then corresponds to the lithium-ion diffusion in the material body impedance phase [35]. The diameter of the HF semicircle of the SiO/G/CNTs composite electrode is much smaller than that of the SiO/G electrode, which indicates that the resistance of former one is much lower. The charge-transfer resistance of SiO/G/CNTs composite particles is 44 Ω, but that of the SiO/G composite particles is 116 Ω, indicating the presence of a small amount of carbon nanotubes in composite materials can make up silicon-based electrodes in embedded lithium initial electronic conductivity is not high enough. More importantly, in the de-embedment process of lithium ion, the volume contraction of the active material particles affects the

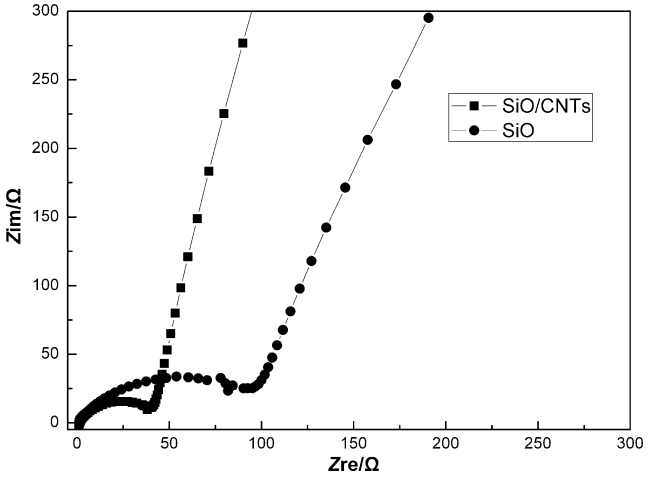

Fig. 7 Electrochemical impedance spectra of SiO/G and SiO/G/CNTs composite electrode before cycling

integrity of conductive network of the electrode with lithium–silicon alloys silicon to a single qualitative change. The existence of carbon nanotubes may provide compensation for electronic conductivity, preventing lithium ion from prolapsing from the lithium–silicon alloys, and then improve the cycle efficiency [36, 37].

Furthermore, EIS was also applied to analyze the evolution of electrode/electrolyte interface. The corresponding Nyquist plots were given in Figs. 8 and 9. Here, R_s is the solution resistance of the cell. R_f and R_{ct} represent the ion transport resistance and anode charge-transfer resistance, respectively. In addition, the sloping line in the lower frequency accords to the lithium-ion diffusion resistance in electrode bulk, namely the Warburg impedance. Non-linear least squares fitting procedure is used to iterate the impedance data applying the inset equivalent circuit in Fig. 8, in which constant phase element (Q) is used to substitute for the

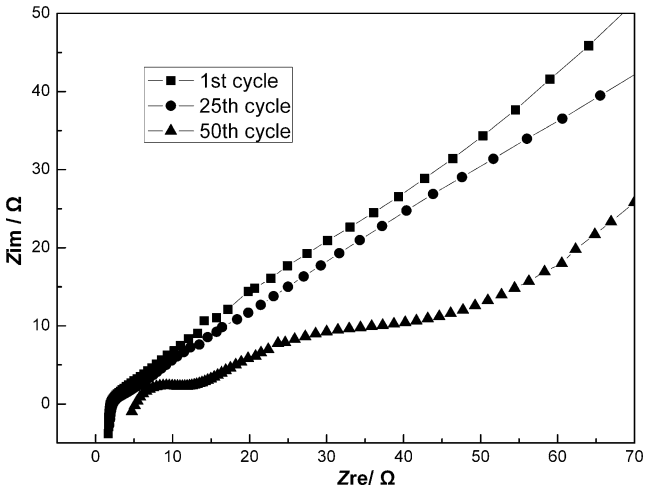

Fig. 8 Electrochemical impedance spectra of SiO/G composite electrode at different stages

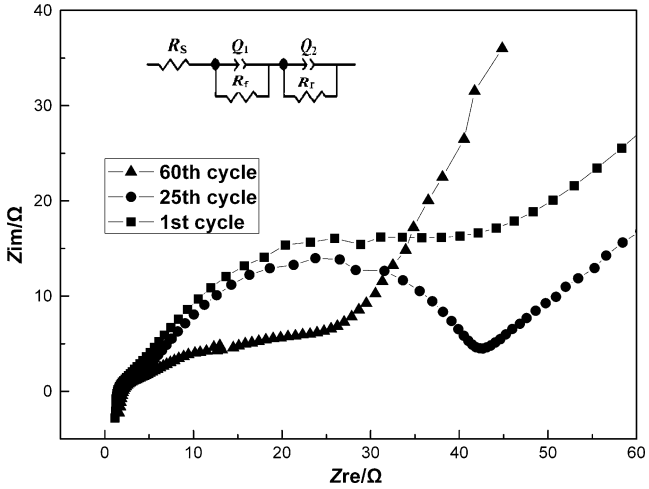

Fig. 9 Electrochemical impedance spectra of CNTs-coated SiO/G electrode at different cycle stage. (*Inset*)The schematic representation of equivalent circuit

capacitance of electric double layer and Warburg impedance for the diffusion effect appearing in Nyquist plots [38], the results are listed in Table 1.

After the first cycle, SiO/G shows only one depressed semicircle in the high and intermediate frequency and a 45° line in the low frequency. With the coating of CNTs, the diameter of the semicircle of SiO/G/CNTs is reduced. A similar phenomenon is observed after 25 and 50/60 charge–discharge cycles, as R_s shown in Table 1. It is reported that the diameter decrease of the semicircle is mainly ascribed to the decrease of the interparticle contact resistance, resulted from the integrity preservation of the conductive network. In general, the R_{ct} and R_f of the SiO/G/CNTs are relatively lower than those of SiO/G. The R_f and Rct of SiO/G after 50 cycles is almost invariable in comparison to that of SiO/G after 1 cycle, while the R_f and R_{ct} of SiO/G/CNTs seriously decreases seriously from the first cycle to the sixtieth cycle. It is suggesting that the conductive network structure of CNT-coated SiO/G is not destroyed and the formed SEI after the first cycle is in favor of the anode charge transfer upon cycling. These results are in good agreement with the SEM images in Fig. 6 and the cycle performance in Fig. 5.

Table 1 Iterated resistances parameters using equivalent circuit in Fig. 9

	SiO/G			SiO/G/CNTs		
	1st	25th	50th	1st	20th	60th
R_s/Ω	3.06	2.89	5.44	2.34	2.47	2.63
R_f/Ω	4.37	2.48	4.18	3.10	1.94	2.09
R_{ct}/Ω	61.71	55.4	61.32	44.16	38.99	16.89

Conclusions

SiO/G/CNTs composite was successfully synthesized by ball milling followed by CVD method in the present study. For comparsion, SiO/G composite was also prepared. The results indicated that SiO/G/CNTs composite showed a higher discharge capacity and a better durability than SiO/G composite. The main reasons for the better electrochemical performance could be attributed to the excellent conductivity and ductility of CNTs matrix, the effective dispersion of SiO/G and the obvious alleviation of SEI on CNTs work.

Acknowledgments A project funded by the Priority Academic Program Development of Jiangsu Higher Education Institutions.

References

1. Naji A, Willmann P, Billaud D (1998) Carbon 36:1347–1352
2. Yamauchi Y, Hino T, Ohzeki K, Kubota Y, Deyama S (2005) Carbon 43:1334–1336
3. Yoon SH, Park CW, Yang HJ, Korai Y, Mochida I, Baker RTK, Rodriguez NM (2004) Carbon 42:21–32
4. Kim YJ, Lee HJ, Lee SW, Cho BW, Park CR (2005) Carbon 43:163–169
5. Dimov N, Kugino S, Yoshio M (2003) Electrochim Acta 48:1579–1587
6. Yang J, Takeda Y, Imanishi N, Capiglia C, Xie JY, Yamamoto O (2002) Solid State Ionics 152–153:125–129
7. Boukamp BA, Lesha GC, Huggins RA (1981) J Electrochem Soc 128:725–729
8. Amezawa K, Yamamoto N, Tomii Y, Lto Y (1998) J Electrochem Soc 145:3313–3319
9. Weydanz WJ, Wohlfahrt-Mehrens M, Huggins RA (1999) J Power Sources 81/82:237–242
10. Larcher D, Mudalige C, George AE, Porter V, Gharghouri M, Dahn JR (1999) Solid State Ionics 122:71–83
11. Lee KL, Jung JY, Lee SW, Moon HS, Park JW (2004) J Power Sources 129:270–274
12. Dimov N, Kugino S, Yoshio M (2004) J Power Sources 136:108–114
13. Yoshio M, Tsumura T, Dimov N (2006) J Power Sources 163:215–218
14. Kim JH, Sohn HJ, Kim H, Jeong G, Choi W (2007) J Power Sources 170:456–459
15. Liu Y, Hanai K, Yang J, Imanishi N, Hirano A, Takeda Y (2004) Solid State Ionics 168:61–68
16. Hanai K, Liu Y, Imanishi N, Hirano A, Matsumura M, Ichikawa T, Takeda Y (2005) J Power Sources 146:156–160
17. Guo ZP, Wang JZ, Liu HK, Dou SX (2005) J Power Sources 146:448–451
18. Wen ZS, Yang J, Wang BF, Wang K, Liu Y (2003) Electrochem Commun 5:165–168
19. Shu J, Li H, Yang R, Shi Y, Huang X (2006) Electrochem Commun 8:51–54
20. Zhang Y, Zhang XG, Zhang HL, Zhao ZG, Li F, Liu C (2006) Electrochim Acta 51:4994–5000
21. Wang W, Kumta PN (2007) J Power Sources 172:650–658
22. Iijima S (1991) Nature 354:56–58
23. Maurin G, Bousquet Ch, Henn F, Bernier P, Almairac R, Simon B (1999) Chem Phys Lett 312:14–18
24. Maurin G, Henn F, Simon B, Colomer JF, Nagy JB (2001) Nano Lett 175–79
25. Frackowiak E, Gautier S, Gaucher H, Bonnamy S, Beguin F (1999) Carbon 37:61–69
26. Ishihara T, Kawahara A, Nishigushi H, Yoshio M, Takita Y (2001) J Power Sources 97/98:822–825
27. Claye AS, Fischer JE, Huffmann CB, Rinzler AG, Smalley RE (2000) J Electrochem Soc 147:2845–2852
28. Gao B, Kleinhammes A, Tang XP, Bower C, Fleming L, Wu Y, Zhou O (1999) Chem Phys Lett 307:153–157
29. Shimoda H, Gao B, Tang XP, Kleinhammes A, Fleming L, Wu Y, Zhou O (2002) Phys Rev Lett 88(1):015502
30. Yu MF, Files BS, Arepalli S, Ruoff RS (2000) Phys Rev Lett 84:5552–5555
31. Thess A, Lee R, Nikolaev P, Dai H, Petit P, Robert J, Xu Ch, Lee YH, Kim SG, Rinzler AG, Colbert DT, Scuseria G, Tománek D, Fischer JE, Smalley RE (1996) Science 273:483–487
32. Demczyk BG, Wang YM, Cumings J, Hetman M, Han W, Zettl A, Ritchie RO (2002) Mater Sci Eng A334:173–178
33. Yang J, Takeda Y, Imanishi N, Capiglia C, Xie JY, Yamamoto O (2002) Solid State Ionics 152(153):125–129
34. Wu X, Wang Z, Chen L, Huang X (2003) Electrochem Commun 5:935–939
35. Wang C, Appleby AJ, Little FE (2001) Electrochim Acta 46:1793–1813
36. Yang XL, Wen ZY, Zhang LL (2007) J Inorg Mater 23:2054–2058
37. Pu WH, Ren JG, Wan CR (2004) J Inorg Mater 19:86–92
38. Guo ZP, Zhao ZW, Liu HK, Dou SX (2005) Carbon 43:1392–1396